RSC Advances

PAPER

View Article Online
View Journal | View Issue

Cite this: *RSC Adv.*, 2026, **16**, 14600

Chemical profiling and sustainable valorization of post-distillation residues of *Vitex rotundifolia*

Kieu Dang Minh Nhut,[a] Dao Pham Duy Quang,[a] Phung Van Trung,[a] Tran Hoai Cuong,[a] Pham Thi Nhat Trinh,*[b] Nguyen Thi Nhu Quynh,[c] Cao Van Du[c] and Le Tien Dung *[a]

Post-distillation residues (PDR) from *Vitex rotundifolia* essential-oil production represent an underutilized biomass stream that can retain medium- and high-polarity constituents. Here, PDR and raw fruits were extracted with 30–96% ethanol under matched ultrasound-assisted extraction conditions and evaluated by TPC/TFC and four bioactivity assays (DPPH, ABTS, NO inhibition, and xanthine oxidase). Among residue-derived extracts, R70 showed the best overall performance (DPPH and ABTS IC_{50} = 24.87 and 24.90 μg mL^{-1}; NO IC_{50} = 104.99 μg mL^{-1}), comparable to the corresponding raw extract (E70; NO IC_{50} = 102.86 μg mL^{-1}). Untargeted UHPLC-QTOF-MS/MS enabled curated tentative annotation of 88 metabolites in R70, dominated by flavonoids, phenolic derivatives, terpenoids, and oxylipins, and four representative known constituents (casticin, quercitrin, vitexilactone, and agnuside) were isolated and structurally confirmed. A comparative greenness screening showed improved mass-based metrics for the residue-based route (PMI/E-factor 1409/1407 *vs.* 1925/1921 for the raw-material route), while per-batch energy-related indicators were higher (climate change 3.63 *vs.* 2.49 kg CO_2-eq), highlighting a material-energy trade-off. Overall, PDR can serve as a viable secondary feedstock for recovering non-volatile bioactive constituents, and the environmental performance of residue valorization is condition-dependent.

Received 13th December 2025
Accepted 2nd March 2026

DOI: 10.1039/d5ra09731b

rsc.li/rsc-advances

1. Introduction

Vitex rotundifolia L. f. is a medicinal shrub widely distributed along coastal regions of Asia and traditionally used for managing headaches, inflammation, menstrual disorders, and respiratory symptoms. Its fruits and leaves contain diverse bioactive constituents – flavonoids, iridoids, diterpenoids, phenolic acids, and volatile terpenes – that have been associated with antioxidant, anti-inflammatory, antimicrobial, and hormone-modulating properties.[1–7] Essential oils from the fruits have been examined for their chemical composition and pharmacological activities;[2,8,9] however, the biomass remaining after hydrodistillation is typically discarded or underutilized despite its potential phytochemical richness.

The post-distillation residue (PDR) represents a major portion of the original plant mass and is expected to retain medium- and high-polarity constituents that do not evaporate during essential-oil extraction. Valorizing this residue aligns with green chemistry and circular-bioeconomy principles, which emphasize resource efficiency, waste reduction, and multi-product recovery.[10–12]

In practice, however, the chemical composition and bioactivity of *V. rotundifolia* residues remain poorly characterized, and no systematic comparison with extracts obtained from raw fruits has been reported.

Most earlier investigations have emphasized essential-oil constituents or extracts from raw fruits, whereas the chemical and sustainability potential of the post-distillation residue remains insufficiently understood. In particular, it is still unclear whether bioactive constituents persist after hydrodistillation, how chemically rich residue-derived extracts are when examined using LC-MS/MS metabolite profiling, and how residue valorization influences material efficiency and energy-related environmental impacts.

To address these issues, we systematically compared extracts obtained from raw fruits and post-distillation residues of *V. rotundifolia* using ethanol at different concentrations. Phenolic content and antioxidant and anti-inflammatory activities were quantified to identify extracts of interest. Untargeted UHPLC-QTOF-MS/MS profiling was performed to map the chemical space of the most active residue extract, followed by isolation and structure elucidation of major constituents. Finally, a greenness assessment incorporating PMI, *E*-factor, and life-cycle-inspired indicators was conducted to evaluate the

[a]*Institute of Advanced Technology, Vietnam Academy of Science and Technology (VAST), 1B TL29, Ho Chi Minh, Vietnam. E-mail: ltdung@iat.vast.vn*

[b]*Department of Natural Science, Tien Giang University, 119 Ap Bac, My Tho, Dong Thap, Vietnam. E-mail: phamthinhattrinh@tgu.edu.vn*

[c]*Faculty of Pharmacy, Lac Hong University, Dong Nai, Vietnam*

sustainability of valorizing PDR as a feedstock for natural-product extraction.

Earlier work on *Vitex rotundifolia* has primarily focused on volatile constituents (essential oils) or extracts prepared directly from raw fruits, whereas the chemical space and bioactivity retained in the post-distillation residue have rarely been examined in a condition-matched manner. In particular, comprehensive LC-MS/MS-based profiling of residue-derived non-volatile metabolites and a side-by-side comparison of residue and raw-material extracts across solvent strengths remain limited in the literature.

In this study, we provide a condition-matched comparison of ethanol extracts from raw fruits and post-distillation residues across 30–96% ethanol, integrating multi-assay bioactivity profiling, untargeted UHPLC-QTOF-MS/MS annotation of the most active residue extract, isolation/structure elucidation of representative constituents, and a life-cycle-inspired, per-batch greenness screening (PMI, *E*-factor and selected impact indicators). This integrated workflow is intended to evaluate residue valorization potential and to identify key material-energy trade-offs, rather than to claim chemical novelty of individual compounds or unconditional environmental superiority.

2. Materials and methods

2.1. Plant material and preparation

Fruits of *Vitex rotundifolia* L. f. were collected from Ninh Thuan Province, Vietnam in September 2024 The sample was identified by Dr Nguyen Thi Thu Hien from Department of Pharmacognosy, Nguyen Tat Thanh university. A voucher specimen was deposited at Department of Technology for Bioactive Natural Products, Institute of Advanced Technology with voucher No 12.2024-Ninh Thuan. After washing, the fruits were shade-dried, followed by oven-drying at 60 °C until moisture content dropped below 12%. The dried fruits were ground into powder and stored in airtight containers. Post-distillation residues (PDR) were similarly air-dried in the shade and subsequently oven-dried to below 15% moisture before extraction.

2.2. Chemicals, reagents and equipment

Solvents and reagents for extraction and chromatography: ethanol 96% (Vietchem, Vietnam), methanol, ethyl acetate, chloroform, and *n*-hexane (Xilong, China).

Chemicals for phytochemical assays: Folin–Ciocalteu reagent (Merck, Germany), gallic acid (99.5%, Merck), quercetin (Merck), aluminum chloride, sodium carbonate, sodium hydroxide, sodium nitrite, sulfuric acid (Xilong, China).

Chemicals for antioxidant assays: 1,1-diphenyl-2-picrylhydrazyl (DPPH, Merck), ABTS (2,2′-azino-bis(3-ethylbenzothiazoline-6-sulfonic acid)), potassium persulfate.

Chemicals for NO inhibition experiment: sulfanilamide and *N*-(1-naphthyl)ethylenediamine dihydrochloride (NED).

Reagents and materials for chromatographic separation: silica gel 60 (Merck), C18 reversed-phase silica gel (Merck), Sephadex LH-20 (Merck), macroporous resin D101.

Other materials: dimethyl sulfoxide (DMSO, Fisher, USA), analytical-grade distilled water, and standard alkanes (C8–C30) for GC–MS retention index calibration.

UV-visible spectrophotometer: UV-1800 (Shimadzu, Japan), used for measuring absorbance in TPC, TFC, DPPH, and ABTS assays.

Gas chromatography–mass spectrometry (GC–MS): GC-2030 system coupled with GCMS-QP2020 detector (Shimadzu, Japan), equipped with Rxi-5MS capillary column (30 m × 0.25 mm, 0.25 μm film thickness), used for essential oil analysis.

Nuclear magnetic resonance (NMR) spectrometer: ^{1}H-NMR (500 MHz) and ^{13}C-NMR (125 MHz), used for structural elucidation of isolated compounds (measured at the Central Analytical Laboratory, Ho Chi Minh City, Vietnam).

2.3. Essential oil distillation and GC–MS analysis

Essential oil was obtained from 200 g of powdered dried fruit by hydrodistillation for 3, 4, and 5 hours using a Clevenger-type apparatus. The oil was dried over anhydrous sodium sulfate and stored at 10 °C. The chemical composition was determined using GC–MS (Shimadzu GC-2030 coupled with GCMS-QP2020) on an Rxi-5MS column (30 m × 0.25 mm, 0.25 μm). Retention indices (RI) were calculated relative to a C8–C30 *n*-alkane series, and compound identification was confirmed by comparison with the NIST 17 MS library and Adams[13] retention index data.

2.4. Extraction procedures

2.4.1 Residue extraction. Post-distillation residues were dried in a ventilated chamber (45 °C) by recovering waste heat from an air-conditioning outdoor unit for 24 h, until moisture content was below 15%. One hundred grams of dried residue were extracted with 1000 mL ethanol at four concentrations (30%, 50%, 70%, and 96%) using ultrasound-assisted extraction (60 °C, 30 min), repeated three times. The UAE temperature (60 °C) and duration (30 min) were selected based on literature precedent for ethanol–water UAE of phenolic-rich plant matrices and practical constraints, aiming to enhance mass transfer while avoiding excessive thermal degradation and unnecessary energy input.[14] The ethanol range (30–96%) was chosen to span polarity and enable a direct, condition-matched comparison between residue and raw materials. Combined filtrates were evaporated under reduced pressure to obtain four extracts: R30, R50, R70, and R96.

2.4.2 Raw material extraction. Raw fruit powder was extracted in parallel using identical conditions and ethanol concentrations to enable direct comparison with residue-derived extracts. Four corresponding extracts (E30, E50, E70, E96) were obtained.

2.5. Phytochemical and biological assays

Total phenolic content (TPC) was determined using the Folin–Ciocalteu method with gallic acid as the standard.[15] Total flavonoid content (TFC) was assessed *via* aluminum chloride colorimetric assay, expressed as quercetin equivalents.[16] Antioxidant activity was evaluated using both $DPPH^{\cdot}$ and $ABTS^{+\cdot}$ radical scavenging assays, following the methods of Blois[17] and Re,[18]

respectively. Nitric oxide (NO) inhibition was assessed in LPS-stimulated RAW264.7 macrophages using the Griess reagent, as described by Green.[19] The murine macrophage cell line RAW264.7 was obtained from the Biotechnology Center of Ho Chi Minh City (Vietnam). Cell viability under the same treatment conditions was evaluated to exclude cytotoxicity-driven apparent NO reduction; NO inhibition was interpreted within concentration ranges maintaining at least 80% viability.[20] For all cell-based experiments, the final DMSO concentration was kept constant (0.5% v/v) and a solvent control was included; dexamethasone was used as a positive control. All measurements were performed in triplicate, and results were reported as mean ± standard deviation (SD). All extractions were performed using a single laboratory batch of feedstock under controlled conditions; thus, batch-to-batch extraction reproducibility was not assessed in the present screening study. Statistical analysis was conducted using one-way ANOVA followed by Tukey's post-hoc test to determine significant differences ($p < 0.05$) between samples, using OriginalPro 2019.

2.6. UHPLC-QTOF-MS/MS acquisition, data processing, and compound annotation

UHPLC-MS analysis was performed using an ExionLC™ UHPLC system (AB SCIEX, USA) coupled to an X500R QTOF mass spectrometer equipped with a Turbo V ion source operating in negative ion mode. Chromatographic separation was achieved on a Hypersil GOLD C18 column (150 × 2.1 mm, 3 μm; Thermo Fisher Scientific, USA) at ambient temperature. The mobile phases consisted of water containing 0.1% formic acid (A) and acetonitrile containing 0.1% formic acid (B), delivered at a flow rate of 0.4 mL min^{-1}. The gradient program was as follows: 0–1 min, 2% (B); 1–30 min, 2–98% (B); 30–36 min, 98% (B). The injection volume was 2 μL.[21,22]

Raw data were processed in SCIEX OS (v1.2.0.4122) for peak detection, alignment, deconvolution, and extraction of precursor/MS/MS spectra. All reported features were supported by MS/MS spectra. Putative annotations were assigned by direct MS/MS library comparison against MoNA and MassBank, accepting candidate precursors within ≤10 ppm. For each library hit, the number of matched diagnostic fragments (*n*_frag) was recorded and used to support a confidence tier; annotations were retained when the MS/MS spectra were chemically interpretable and showed library-consistent fragment evidence.[23] All assignments are reported as putative identifications (MSI level 2).[24] To improve transparency and mitigate false positives, an internal confidence tier was applied: high ($|\Delta ppm| \leq 5$ and $n\_frag \geq 8$), medium ($|\Delta ppm| \leq 10$ and $n\_frag = 4–7$), and low ($|\Delta ppm| \leq 10$ and $n\_frag < 4$). These annotations provide dereplication-level chemical context and are not intended as definitive identification or quantification. For each annotated feature, Δppm, *n*_frag, and confidence tier are reported in Table S4.

2.7. Fractionation and isolation

The 70% ethanol extract from the post-distillation residue (R70), which exhibited the highest bioactivities, was selected for isolation. The VR-R70 extract (14.3 g) was subjected to column chromatography on silica gel, eluted sequentially with *n*-hexane, *n*-hexane:ethyl acetate (1 : 1), ethyl acetate, and methanol. This process yielded four fractions: the *n*-hexane fraction (VRH, 3.92 g), the *n*-hexane:ethyl acetate fraction (VRHEA, 5.67 g), the ethyl acetate fraction (VREA, 2.05 g), and the methanol fraction (VRM, 2.69 g).

The VRHEA fraction (5.67 g) was further fractionated on a normal-phase silica gel column using a gradient elution of *n*-hexane and ethyl acetate (from 9 : 1 to 6 : 4, v/v). Eight subfractions were obtained (VRHEA1- 8), among which VRHEA5 (144.1 mg) and VRHEA2 (357.5 mg), showing well-resolved spots on TLC, were selected for further purification. Compound **VR1** (87.2 mg) was crystallized directly from VRHEA5. VRHEA2 underwent successive purification steps using silica gel columns with *n*-hexane:ethyl acetate and chloroform:methanol systems, ultimately yielding compound **VR2** (13.7 mg).

The methanol-soluble fraction (VRM, 2.69 g) was fractionated on a D101 macroporous resin column using a gradient elution from water to 100% methanol, resulting in five subfractions: VRM1 (5342.2 mg), VRM2 (640.3 mg), VRM3 (850 mg), VRM4 (612.8 mg), and VRM5 (146.4 mg). VRM3 was further processed by silica gel column chromatography, from which subfraction VRM3.5 was purified using Sephadex LH-20 (MeOH 100% as eluent), followed by reversed-phase silica gel chromatography (MeOH–H_2O = 1 : 2, v/v) to yield compound **VR3** (19.5 mg). Similarly, VRM3.4 was separated on Sephadex® LH-20 eluting with MeOH to obtain compound **VR4** (48.1 mg).

All isolated compounds (**VR1–VR4**) were monitored for purity by thin-layer chromatography using multiple solvent systems and visualized under UV light or by sulfuric acid staining. The structures of the four isolated constituents were established from their full NMR spectrum (Fig. S1–S8) and verified by comparison with literature-reported NMR values.

2.8. Environmental assessment (comparative, life-cycle-inspired screening; per-batch)

We performed a comparative, life-cycle-inspired screening at lab scale to contrast Route A and Route B on the same per-batch basis (identical input mass and laboratory scale).

Assumptions and limitations. Because the target marker content in PDR was not quantified, no product-based functional unit (*e.g.*, per gram of casticin) was applied; therefore, the environmental indicators are reported as per-batch, process-level comparisons. Electricity consumption was calculated from equipment rated power and operating time for each unit operation, and solvent losses were estimated based on measured volumes before and after recovery steps. To improve transparency, the inventory assumptions (electricity, solvent use and losses) are summarized in the SI, and a brief scenario check is provided to illustrate how solvent-recovery and energy-integration assumptions influence the direction and magnitude of the results.[25–27]

Additional inventory transparency (screening-level): the full process-step inventory of electricity, water and ethanol inputs for Route A and Route B is reported in Tables S7A–S7C.

Transport distances were not included at this screening level, and no stochastic uncertainty analysis was performed; instead, a simple ±20% scenario check (electricity and solvent recovery/loss) is provided in Table S7C to illustrate robustness of comparative trends.

2.9. Processing and analyzing statistics

All statistical analyses (univariate and multivariate), curve fitting and data visualization were performed in OriginPro 2019 (OriginLab Corp., Northampton, MA, USA). Unless otherwise specified, data are expressed as mean ± standard deviation (SD) from technical triplicates ($n = 3$).

Concentration – response data for antioxidant (DPPH, ABTS) and enzyme/inflammation assays (XO, NO) were analyzed by non-linear regression using OriginPro 2019 for IC_{50} estimation. Multiple-group comparisons used one-way ANOVA followed by Tukey's HSD post-hoc test. Pairwise comparisons (when applicable) used two-tailed Student's *t*-test. Statistical significance was set at $p < 0.05$. PCA and Pearson correlation coefficients (r) were performed in OriginPro 2019. LCA inventories were compiled per batch and characterized using Mobius with EF 3.1 characterization factors.

3. Results and discussion

3.1. Essential oil composition

Essential oil from *V. rotundifolia* fruits was obtained by hydrodistillation for 3, 4, and 5 h to generate the post-distillation residue (PDR) used in this study. The oil yield increased from 0.43 mL per 200 g (3 h) to 0.62 mL per 200 g (5 h), and GC–MS analysis indicated a time-dependent shift in volatile composition (Table 1).

As hydrodistillation primarily removes volatile constituents, the resulting residue is expected to retain non-volatile metabolites, providing the rationale for the subsequent comparative extraction, bioactivity screening, and LC-MS/MS dereplication of the PDR. The essential-oil composition and antibacterial screening results (Tables 1 and 2) are included solely to document the distillation step and to describe the volatile fraction removed during processing. No causal linkage between individual volatile constituents and antibacterial effects is inferred in the present study; the main focus is the non-volatile fraction retained in PDR and its recovery under the tested extraction conditions.

Table 2 Antibacterial activity (inhibition zones, mm) of essential oils against *S. aureus* and MRSA[a]

Sample	*S. aureus* (mm)	MRSA (mm)
EO3	8.2 ± 0.1	5.2 ± 0.2
EO4	8.1 ± 0.2	9.1 ± 0.1
EO5	14.9 ± 0.1	4.7 ± 0.2
Gentamicin	21.6 ± 0.2	22.1 ± 0.2
DMSO 100%	0.0	0.0

[a] Values represent the average diameter (mm) of the inhibition zone against tested bacteria ($n = 4$). Larger diameters indicate stronger antibacterial activity.

3.2. Phytochemical content and antioxidant activity of ethanol extracts from raw and residual material

Ethanol extracts were prepared from both raw *V. rotundifolia* fruits (E30–E96) and post-distillation residues (R30–R96) using four solvent concentrations (30%, 50%, 70%, and 96%). Total phenolic content (TPC), total flavonoid content (TFC), and antioxidant and anti-inflammatory activities (DPPH, ABTS, NO, and XO inhibition) were quantified to evaluate the retention and recovery of bioactive constituents in the residue matrix. Results are summarized in Table 3.

Across all extraction conditions, raw-material extracts generally exhibited higher TPC and TFC than residue-derived samples. Among them, E96 yielded the highest phenolic (159.38 mg GAE per g) and flavonoid content (451.73 mg QE per

Table 1 Major volatile constituents of *V. rotundifolia* essential oil at 3, 4, and 5 hours[a]

	RI			Content (%)		
RT (min)	Adam	Cacld.	Compound	EO3	EO4	EO5
7.633	932	926	α-Pinene	0	0	5.69
12.86	1026	1025	1,8-Cineole	0	0	3.00
28.792	1346	1344	α-Terpinyl acetate	12.20	5.90	8.56
31.019	1417	1415	*trans*-Caryophyllene	1.24	0.67	1.13
33.668	1452	1461	α-Humulene	0.96	0.59	0.91
33.81	1522	1517	δ-Cadinene	1.42	0.81	1.39
40.001	1649	1643	*cis*-Guaia-3,9-dien-11-ol	6.70	6.49	0
40.146	1749	1751	α-Bisabolol oxide A	3.97	3.98	3.74
40.319	1987	1982	Manool oxide	21.35	21.74	18.44
40.784	2043	2045	Kaurene	9.33	8.89	16.50
40.99	2184	2184	Sandaracopimarinal	18.94	18.93	10.29
41.188	n.a	2573	4,16-Androstadien-3-one	1.65	1.58	2.79
Oxygenated compounds				**53.34**	**56.04**	**49.08**
Non-oxygenated compounds				**44.67**	**41.95**	**49.64**

[a] Only compounds with content >1% in at least one distillation time or relevant to bioactivity (*e.g.*, α-pinene, 1,8-cineole) are listed. RT = retention time. Detail compounds was shown in Table S1.

Table 3 Total phenolic content (TPC), total flavonoid content (TFC), and antioxidant activity (IC_{50} of DPPH and ABTS assays), nitric oxide, xanthine oxidase inhibition of ethanol extracts from *V. rotundifolia* raw material (E-serie samples) and post-distillation residue (R-serie samples)[a]

Sample	Source	EtOH (%)	Yield (%)	TPC (mg GAE per g)	TFC (mg QE per g)	IC_{50} (μg mL^{-1}) DPPH	ABTS	NO	XO
R30	Residue	30	11.84	97.55	239.99	43.79	65.51	142.14	193.18
R50	Residue	50	10.91	109.39	298.90	27.74	29.54	150.93	182.24
R70	Residue	70	10.53	149.03	413.97	24.87	24.90	104.99	146.86
R96	Residue	96	9.69	100.43	179.48	62.50	76.32	184.03	117.62
E30	Raw	30	8.67	100.00	269.72	39.04	46.92	120.15	196.58
E50	Raw	50	7.08	136.69	351.66	27.91	40.73	141.85	188.16
E70	Raw	70	6.69	155.67	426.29	25.26	28.35	102.86	138.07
E96	Raw	96	7.54	159.38	451.73	22.71	25.38	92.70	108.77
Vitamin C						5.37			
Trolox							2.87		
Dexamethasone								0.49	
Allopurinol									1.68

[a] TPC = Total phenolic content (mg gallic acid equivalents per gram dry extract); TFC = Total flavonoid content (mg quercetin equivalents per gram); DPPH, ABTS = Antioxidant activity; NO: nitric oxide; XO: xanthine oxidase; values are mean of 3 replicates.

g), whereas R70 represented the strongest extract from the residue series (TPC: 149.03 mg GAE per g; TFC: 413.97 mg QE per g). These results confirm that although essential-oil distillation removes volatile constituents, substantial amounts of medium- and high-polarity phytochemicals remain available for recovery.

Antioxidant activities showed a similar pattern. R70 displayed the strongest activity among residue extracts (DPPH IC_{50} = 24.87 μg mL^{-1}; ABTS IC_{50} = 24.90 μg mL^{-1}), whereas E96 remained the most potent overall (22.71 μg mL^{-1} and 25.38 μg mL^{-1}, respectively). As noted previously,[28–30] the antioxidant capacity does not always scale proportionally with TPC/TFC, indicating the influence of compound subclass distribution and structural features.

Cell viability assays in RAW264.7 cells indicated that all extracts maintained ≥80% viability up to 200 μg mL^{-1}, while moderate cytotoxicity was observed at 400 μg mL^{-1} for selected samples (Table S6); NO inhibition was therefore interpreted within non-cytotoxic concentration ranges.

To explore relationships among extracts, PCA was conducted using six normalized variables (TPC, TFC, DPPH, ABTS, NO, XO). The score plot (Fig. 1A) suggests that R70 and E70 have broadly similar phytochemical and bioactivity profiles, whereas E96 is positioned separately, consistent with its high phenolic/flavonoid content. Given the limited number of samples, the PCA is used here as an exploratory visualization rather than a definitive classification model.

In the biplot (Fig. 1B), PC1 (68.12%) largely reflects covariation between TPC/TFC and the antioxidant/NO variables, while PC2 (17.71%) is influenced more strongly by XO inhibition. These loading patterns indicate that XO behaves partly independently from the other assays under the tested conditions.

Pairwise relationships were further examined using Pearson correlation analysis (Fig. 2 and Table S3). TPC and TFC

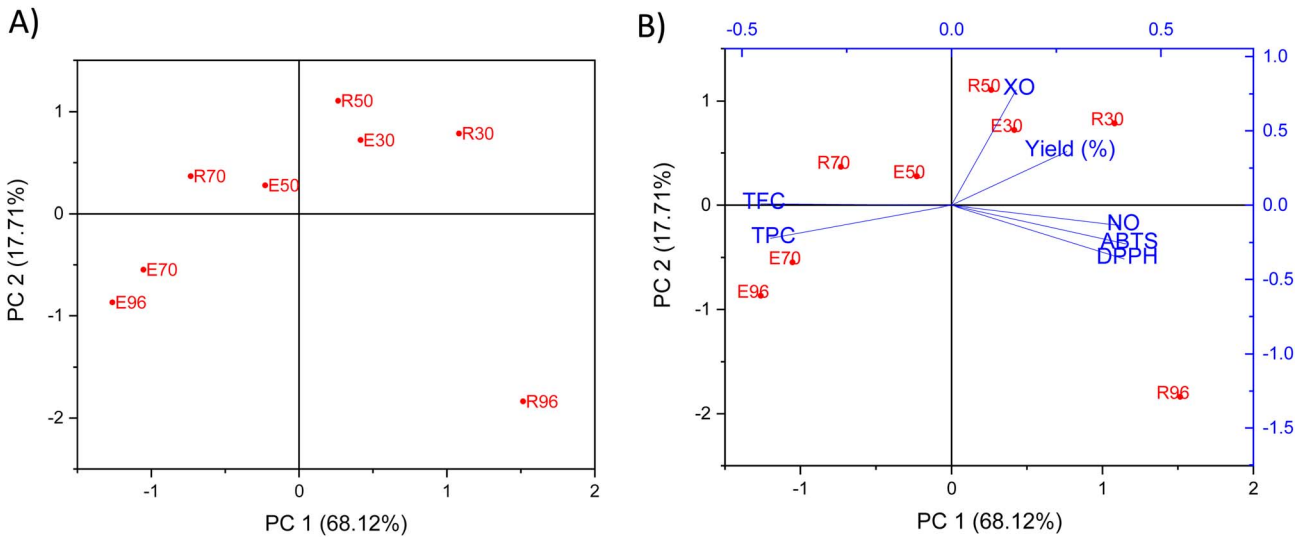

Fig. 1 Principal component analysis (PCA) of extract phytochemical and bioactivity variables. PC1 = 68.12%, PC2 = 17.71%. (A): PCA score plot. (B): PCA biplot.

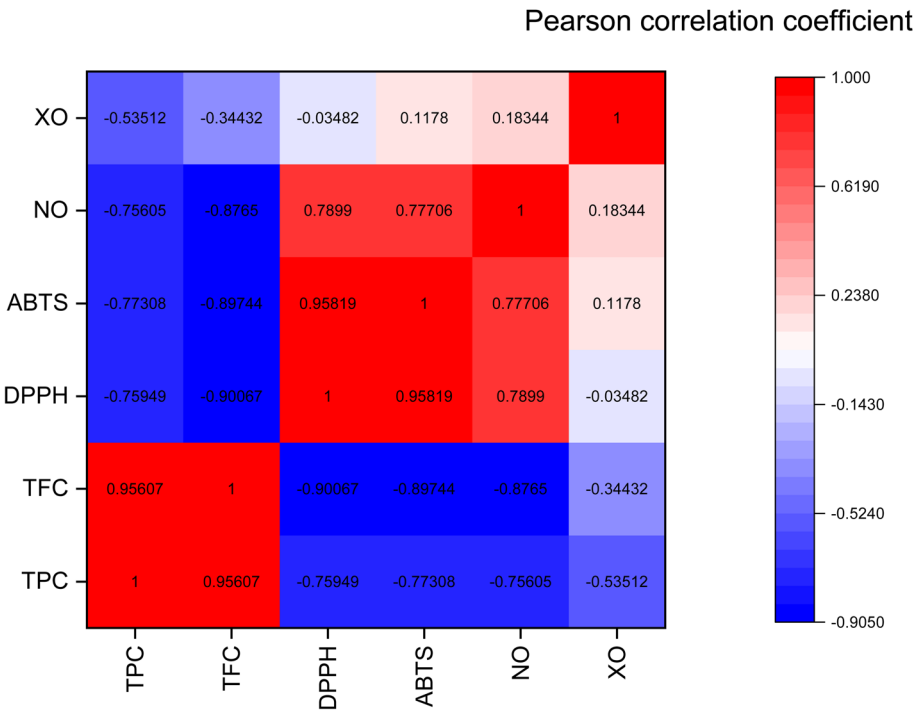

Fig. 2 Pearson correlation heatmap with two-tailed significance values ($p < 0.05$). Color scale indicates correlation strength.

correlated strongly and negatively with DPPH ($r = -0.76, -0.90$) and ABTS ($r = -0.77, -0.90$). Moderate correlations were also observed with NO inhibition, whereas XO inhibition showed weak or nonsignificant correlations ($r < 0.35$).

Together, these exploratory multivariate and correlation analyses support selecting R70 as a balanced residue-derived extract under the tested solvent conditions for subsequent chemical profiling and isolation, while acknowledging that broader validation across independent batches would be required for predictive modeling.[31–33]

3.3. LC-MS/MS profiling of the R70 extract

3.3.1 Feature detection and annotation confidence. Untargeted UHPLC-QTOF-MS/MS analysis of the R70 extract enabled the tentative annotation of 88 metabolites (Tables 4 and S4). All reported features were supported by MS/MS spectra and assigned as putative identifications (MSI level 2) based on accurate precursor mass (≤10 ppm) and direct spectral comparison with reference MS/MS libraries (MoNA and MassBank).

To improve transparency and mitigate potential false positives, an internal confidence tier was applied based on mass accuracy and the number of matched diagnostic fragments: high ($|\Delta ppm| \leq 5$ and $n\_frag \geq 8$), medium ($|\Delta ppm| \leq 10$ and $n\_frag = 4–7$), and low ($|\Delta ppm| \leq 10$ and $n\_frag < 4$). For each annotated feature, Δppm, n_frag, and confidence tier are reported in Table S4.

All annotations are reported at MSI level 2 and are intended to provide dereplication-level chemical context rather than definitive structural confirmation or quantification, in accordance with established reporting recommendations for non-targeted LC-MS workflows.[23,34,35]

Table S4 represents a curated subset of chemically interpretable and class-consistent features. Signals with low-quality MS/MS spectra or conflicting library matches were excluded to enhance annotation robustness.

3.3.2 Chemical composition overview. Based on the curated annotations (Table S4), the R70 extract comprised 88 putatively identified metabolites spanning multiple chemical

Table 4 Representative annotated compounds from R70 based on LC-MS/MS

No.	Compound	m/z $[M–H]^-$	m/z_calc	Error ppm	Matched fragments	Key fragments
1	3,4-Dihydroxybenzoic acid	153.0193	153.0193	0.12	31	109.029; 80.026; 65.039
2	Trihydroxyoctadecadienoic acid (oxylipin)	327.2177	327.2176	0.04	34	309.206; 291.195; 171.102
3	Polyhydroxylated tetradecahydropicene	503.3349	503.3378	−5.68	34	485.324; 457.327; 71.012
4	Hexacyclic diterpenoid dicarboxylic acid	485.3265	485.3260	0.05	11	94.98; 80.96; 59.01; 151
5	Monoterpenoid bicyclic	293.1744	293.1758	−4.67	15	59.013; 61.987; 192.114
6	Furan–spiro-oxolane diterpenoid	361.1659	361.1656	0.66	28	299.165; 343.962; 57–67
7	Caffeoyl quinic acid isomer	191.0556	191.0561	−2.18	27	191; 85–127
8	Quercetin	301.0347	301.0353	−1.99	111	151.001; 179.006

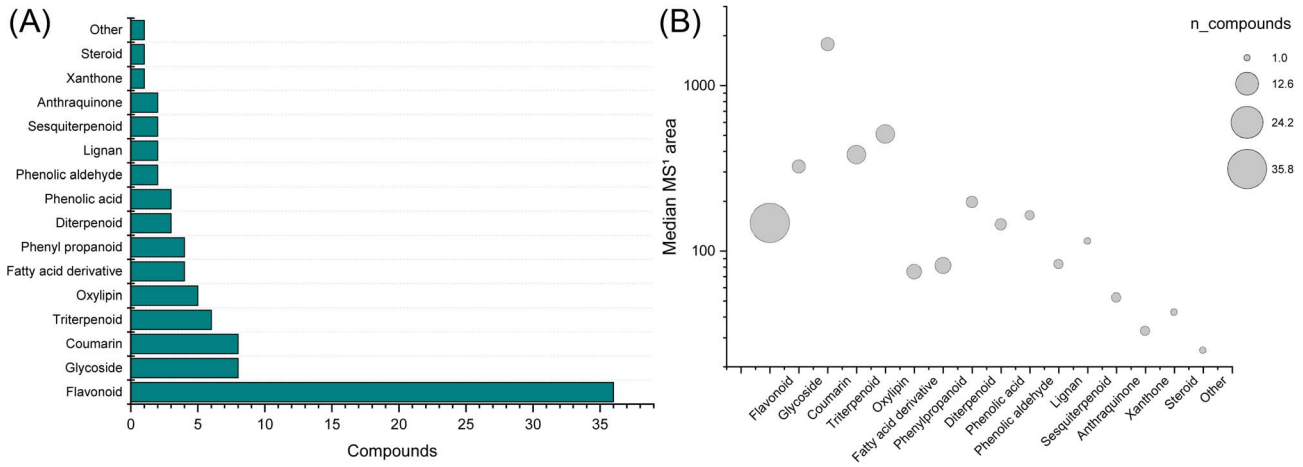

Fig. 3 (A). Distribution of annotated metabolites in the R70 extract according to chemical classes based on UHPLC-QTOF-MS/MS analysis. Flavonoids represent the dominant class, followed by terpenoids and phenolic derivatives. (B) Bubble plot illustrating the distribution of annotated metabolites across chemical classes. The y-axis represents the median MS^1 peak area (log scale), while bubble areas are proportional to the number of compounds identified in each class.

classes (Fig. 3A). Flavonoids represented the largest group (35 compounds, 40%), followed by phenolic derivatives (17 compounds, 19%), terpenoids (13 compounds, 15%), oxylipins and fatty-acid derivatives (13 compounds, 15%), and other minor classes (10 compounds, 11%).

The relative class distribution is consistent with previous phytochemical reports on *Vitex rotundifolia*, which describe flavonoids, iridoids, and terpenoid derivatives as major constituents of the species.[36–39] Notably, despite hydrodistillation removing volatile monoterpenes and sesquiterpenes, a diverse spectrum of non-volatile phenolic and terpenoid metabolites remained detectable in the post-distillation residue.

This retained chemical diversity is consistent with the observed extract-level antioxidant and NO-inhibitory screening activities and supports the feasibility of recovering bioactivity-relevant metabolite classes from PDR.

3.3.3 Bioactivity-relevant metabolite classes. Flavonoids constituted the most abundant and structurally diverse class, including flavones, flavonols, and their glycosides (*e.g.*, quercetin-, kaempferol-, luteolin-, and isovitexin-type derivatives). MS/MS spectra displayed characteristic retro-Diels-Alder (RDA) fragmentation and neutral losses of hexose (162 Da) or deoxyhexose (146 Da), consistent with established fragmentation patterns for flavonoid glycosides.[40]

Seventeen phenolic-type metabolites were annotated, including simple phenolic acids and caffeoylquinic acid derivatives. Such phenolic structures are widely associated with antioxidant capacity in plant extracts.[15,28]

Thirteen non-volatile terpenoid metabolites were identified, including diterpenoid and triterpenoid derivatives previously reported in *Vitex* species.[5] Their detection after hydrodistillation indicates that structurally complex, less-volatile constituents persist in the residue matrix.

Additionally, several oxylipins and hydroxy fatty-acid derivatives were observed. These lipid-derived metabolites have been increasingly recognized as plant signaling molecules and may contribute to extract-level bioactivity profiles.[41]

Collectively, these metabolite classes represent well-documented phytochemical constituents of *Vitex rotundifolia*, and their presence in the PDR extract indicates that essential-oil removal does not exhaust the non-volatile chemical space of the material.

3.3.4 Valorization significance and limitations. The LC-MS/MS data demonstrate that the post-distillation residue retains a chemically diverse set of bioactivity-relevant metabolite classes dominated by flavonoids, phenolic derivatives, and non-volatile terpenoids. Importantly, these compounds correspond to known phytochemical features of *Vitex* species rather than novel chemical entities.

Accordingly, the present profiling is intended to confirm the recoverability and compositional continuity of established metabolite classes in PDR, rather than to claim structural novelty. In combination with extract-level bioactivity screening and process-level environmental assessment, these data support the feasibility of valorizing post-distillation biomass as a secondary feedstock within circular extraction strategies, while acknowledging that compound-level quantification and mechanistic validation would require further investigation.

Collectively, the LC-MS/MS dereplication indicates that non-volatile, bioactivity-relevant metabolite classes persist in PDR after hydrodistillation, supporting feasibility of secondary-feedstock recovery rather than demonstrating mechanistic causality or chemical novelty.

3.4. Isolation, structural elucidation, and bioactivity of compounds from R70

Guided by the LC-MS/MS metabolite profile (Section 3.3), which indicated enrichment in flavonoids, diterpenoids, and iridoid glycosides, the R70 extract was prioritized for isolation. R70 displayed strong antioxidant activity (DPPH IC_{50} = 24.87 μg mL^{-1}; ABTS IC_{50} = 24.90 μg mL^{-1}) and effective NO inhibition, making it an appropriate target for bioactivity-guided

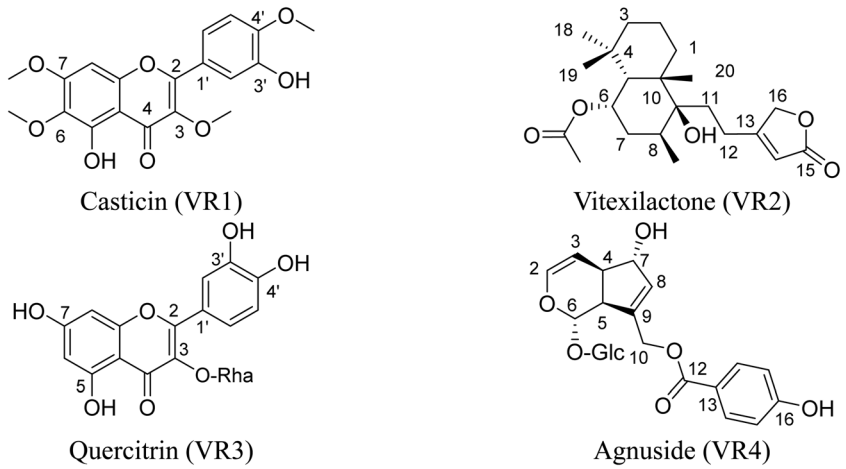

Fig. 4 Chemical structures of compounds isolated from R70 (**VR1–VR4**).

fractionation. Chromatographic purification of VRHEA and VRM fractions yielded four major constituents (**VR1–VR4**), identified as casticin, vitexilactone, quercitrin, and agnuside (Fig. 4).

Compound **VR1** (87.2 mg) was obtained from VRHEA5. Its ^{13}C-NMR spectrum showed 19 carbon signals, including four methoxy carbons (55–60 ppm) and a characteristic C-4 carbonyl (178.97 ppm). The ^{1}H-NMR displayed aromatic protons between 6.5–8.0 ppm and a diagnostic singlet at 6.51 ppm (H-8), indicating substitution on C-5/C-6/C-7. An ABX coupling system at 7.72, 6.96, 7.68 ppm matched H-6′, H-5′, H-2′ of a 3′,4′-disubstituted B-ring. Four methoxy singlets (3.88–3.99 ppm) showed HMBC correlations confirming substitution at C-4′, C-7, C-3, C-6. Additional HMBC correlations between H-6′ with C-2/C-4′; H-8 with C-6/C-7/C-9/C-10 reinforced the structure. The NMR data were entirely consistent with published values for casticin.[42]

Compound **VR2** (13.7 mg) from VRHEA2 showed four methyl singlets (0.93–1.03 ppm), typical for a labdane skeleton. The ^{1}H-NMR displayed resonances at δ 4.78 and 5.86 ppm, characteristic of methylene and olefinic protons in an α,β-unsaturated γ-lactone. A signal at δ 5.83 collapsed under selective decoupling, confirming coupling within the lactone system. The ^{13}C-NMR revealed 22 carbons, including γ-lactone signals at δ 174.0, 170.9, 73.1, and an acetoxyl group. The combined spectral features matched literature data for vitexilactone.[36]

The ^{1}H NMR spectrum of compound **VR3** (19.5 mg) showed four downfield OH singlets (>9 ppm) and an ABX pattern at 6.86–7.30 ppm corresponding to B-ring protons. H-6 and H-8 doublets (6.20, 6.38 ppm, J = 2.0 Hz) indicated a 5,7-disubstituted A-ring. Sugar signals included an anomeric proton at 5.25 ppm (J = 1.5 Hz), confirming α-L-rhamnose, and a methyl carbon at 17.44 ppm. The ^{13}C-NMR showed 21 carbons consistent with a flavonol glycoside. The data matched published NMR for quercitrin.[43]

VR4 (48.1 mg) exhibited hallmark iridoid signals in ^{1}H NMR spectrum: δ 6.36 (H-3) and 5.13 (H-4) for an enol/olefin pair,

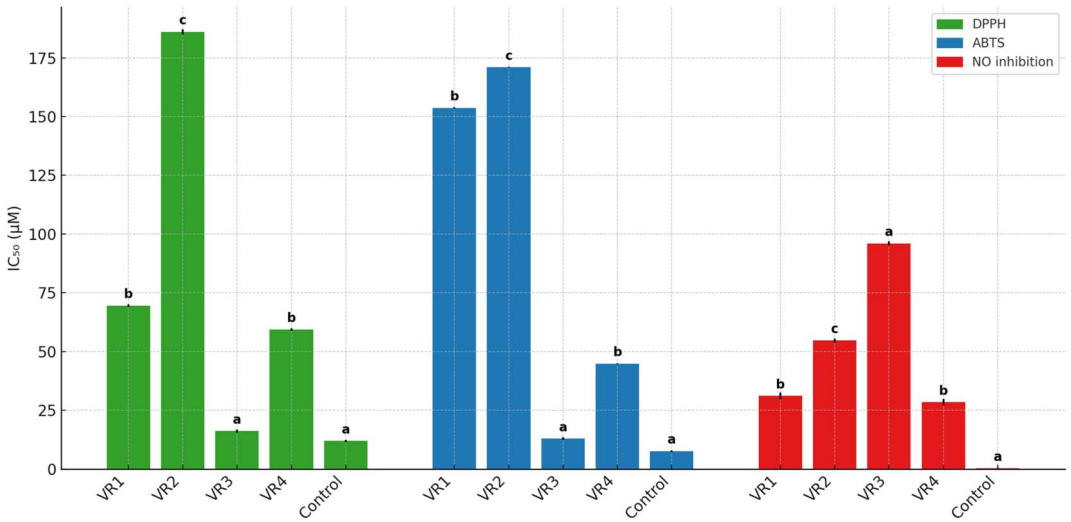

Fig. 5 IC_{50} values of isolated compounds and reference standards in DPPH, ABTS, and NO inhibition assays (n = 3). Bars with different letters (a, b and c) within each assay indicate significant differences (p < 0.05).

with singlets at 5.85 and 6.37 ppm (H-7, H-10). Sugar signals (3.38–3.88 ppm) included δ 4.73 (H-1′, J = 8 Hz), indicating β-glucopyranoside. Aromatic protons at 6.88 and 7.96 ppm suggested a caffeoyl moiety. The ^{13}C-NMR spectrum showed characteristic iridoid carbons and ester carbonyls. NMR data were fully consistent with literature reports for agnuside.[6]

Antioxidant and NO-inhibitory effects of **VR1–VR4** are presented in Fig. 5. **VR3** (quercitrin) exhibited the strongest antioxidant capacity (ABTS IC_{50} = 12.76 μM; DPPH IC_{50} = 16.05 μM), consistent with the radical-scavenging properties of polyhydroxylated flavonols.[44] **VR1** (casticin) and **VR4** (agnuside) exhibited the strongest NO inhibition (IC_{50} = 31.05 and 28.41 μM), reflecting their ability to modulate inflammatory pathways.[45,46] **VR2** displayed moderate activities.

Bioactivities of natural isolates were lower than dexamethasone (IC_{50} = 0.49 μM), but **VR3** showed antioxidant potency comparable to quercetin and superior to vitamin C.[47]

Collectively, these data indicate that R70 owes much of its bioactivity to its flavonoid and iridoid constituents. While the isolated compounds are well-known metabolites previously reported from *Vitex* species, their recovery from the post-distillation residue matrix demonstrates that PDR can retain and serve as a practical secondary source of representative bioactive constituents after essential oil removal.

3.5. Environmental assessment and greenness metrics (per-batch)

Casticin was selected as the representative marker for environmental evaluation because it is a major bioactive flavonoid present in both raw and residue extracts of *V. rotundifolia*,[4,39,48] with well-documented anti-inflammatory, anticancer, and antioxidant activities.[3,49] Evaluating the sustainability of its isolation therefore reflects both pharmacological relevance and practical feasibility. To enable a fair comparison without quantifying marker content in residues, all environmental indicators were assessed per batch rather than per gram of purified compound (Fig. 6).

3.5.1 Life-cycle-inspired screening (per-batch impacts). A comparative LCA was conducted between Route A (raw material extraction) and Route B (post-distillation residue extraction), using system boundaries shown in Fig. 7. Key impacts – including climate change, fossil resource use, water consumption, and acidification – are presented in Tables 5 and 6 and visualized in Fig. 8. Technical differences between routes, including reduced solvent and shorter extraction time in ultrasound-assisted extraction (UAE), are illustrated in Fig. 6.

Route A generated a total climate change impact of 2.49 kg CO_2-eq, whereas Route B reached 3.63 kg CO_2-eq per batch. The higher burden in Route B was driven primarily by increased electricity and ethanol requirements during re-extraction,

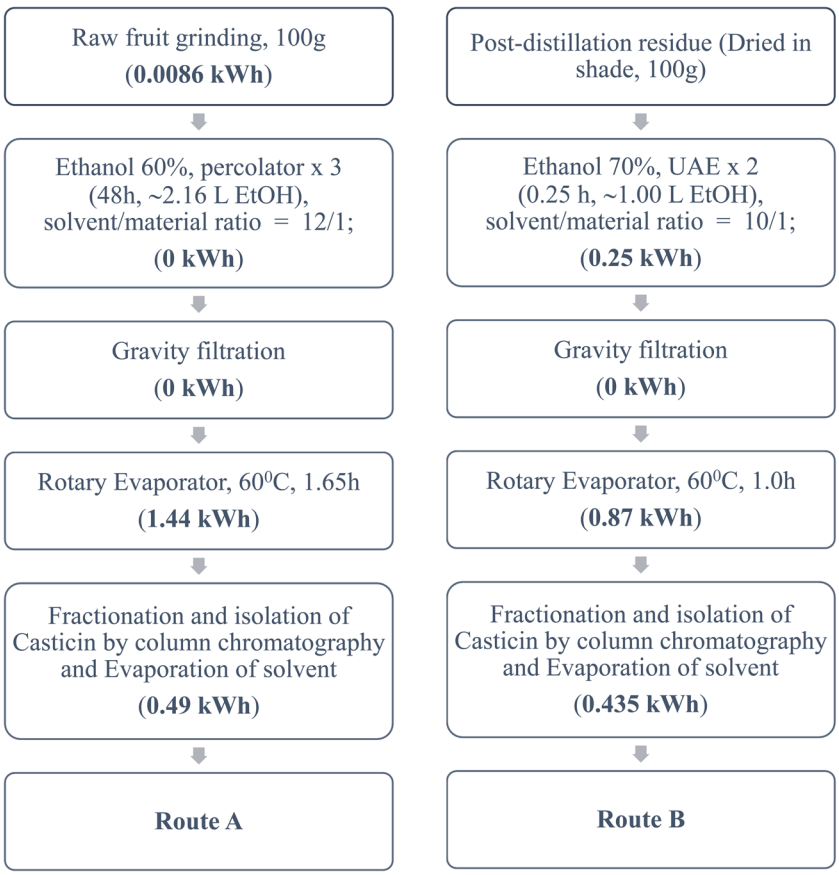

Fig. 6 Schematic comparison between Route A (maceration from raw material) and Route B (ultrasound-assisted extraction from post-distillation residue), illustrating solvent usage, processing time, and energy input at each step.

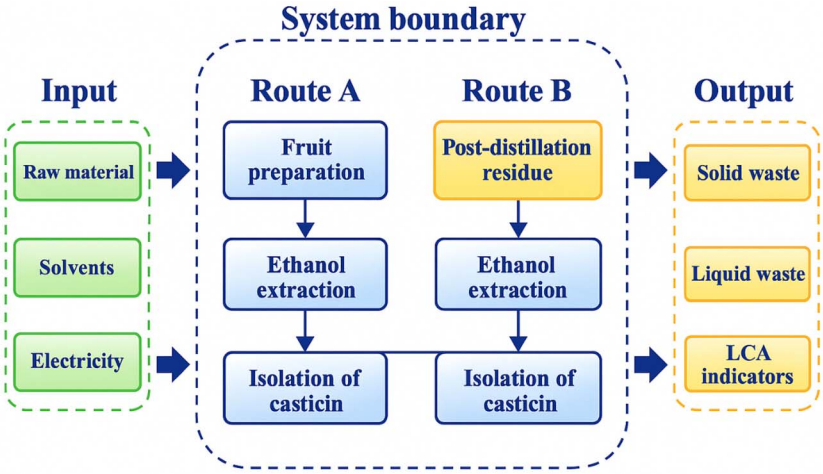

Fig. 7 System boundary diagram comparing two isolation processes of casticin: Route A from raw material and Route B from post-distillation residue. Inputs include raw material (Route A only), solvents, and electricity. Outputs comprise solid waste, liquid waste, and life cycle assessment (LCA) indicators. Route A was adapted from (Hu *et al.*, 2007),[50] while Route B corresponds to the present work.

consistent with prior observations that valorizing waste streams may increase energy demand unless optimized.[51,52]

Fossil-derived emissions also followed this trend (2.83 *vs.* 1.94 kg CO_2-eq). Biogenic emissions were higher in Route B (0.65 *vs.* 0.45 kg CO_2-eq), reflecting the organic load remaining in residues, in agreement with earlier studies reporting substantial biogenic fractions in post-distillation biomass.[53–55]

Route B also required more water (3.67 *vs.* 2.88 m^3), mainly due to ethanol dilution and washing operations, a trend consistent with hydrophilic solvent systems in green extraction workflows.[56] Acidification potential similarly increased (0.022 *vs.* 0.015 mol H^+-eq), largely linked to electricity and ethanol production. Although UAE shortens extraction time and reduces solvent,[56,57] its electricity demand contributes to the LCA footprint. Renewable or hybrid energy integration (*e.g.*, solar-UAE) could mitigate this burden.

Route B consumed 97.35 MJ of fossil energy, compared to 65.63 MJ in Route A. This illustrates the classic green-chemistry trade-off between circularity and processing intensity:[12] although Route B avoids harvesting fresh biomass, the benefit is partly offset by energy needs. Still, Route B aligns with several principles of green chemistry,[10] including prevention, renewable feedstocks, and – when optimized – energy efficiency.

Table 5 Per-batch environmental indicators for Route A *vs.* Route B

Impact category	Unit	Route A	Route B
Acidification	mol H^+ eq	0.015158	0.02245088
Climate change	kg CO_2-eq	2.493344	3.626899
Climate change – biogenic	kg CO_2-eq	0.448918	0.6509545
Climate change – fossil	kg CO_2-eq	1.93927	2.825364
Climate change – land use and LU change	kg CO_2-eq	0.105182	0.1505962
Ecotoxicity, freshwater	CTUe	0.0432112	0.0621488
Ecotoxicity, freshwater – inorganics	CTUe	0.024813	0.0355113
Ecotoxicity, freshwater – organics	CTUe	0.0183982	0.0266375
Eutrophication, freshwater	kg P eq	0.00367948	0.00548383
Eutrophication, marine	kg N eq	0.00581644	0.00865242
Eutrophication, terrestrial	mol N eq	0.0476776	0.0693922
Human toxicity, cancer	CTUh	3.05×10^{-6}	4.30×10^{-6}
Human toxicity, cancer – inorganics	CTUh	2.16×10^{-6}	3.04×10^{-6}
Human toxicity, cancer – organics	CTUh	8.91×10^{-7}	1.26×10^{-6}
Human toxicity, non-cancer	CTUh	8.79×10^{-6}	1.26×10^{-5}
Human toxicity, non-cancer – inorganics	CTUh	5.10×10^{-6}	7.29×10^{-6}
Human toxicity, non-cancer – organics	CTUh	3.68×10^{-6}	5.31×10^{-6}
Ionising radiation	kBq U235 eq	0.00758526	0.01028072
Land use	Pt	4.3635	6.2219
Ozone depletion	kg CFC-11 eq	1.91×10^{-6}	2.71×10^{-6}
Particulate matter	kg PM2.5 eq	0.000585124	0.000835195
Photochemical ozone formation	kg NMVOC eq	0.006673	0.009448905
Resource use, fossils	MJ	65.63016	97.35076
Resource use, minerals and metals	kg Sb eq	0.00438966	0.00582282
Water use	m^3	1.99894	3.079166

Table 6 Key impact factors

Impact category	Unit	Route A	Route B
Acidification	mol H^+ eq	0.015158	0.022451
Climate change	kg CO_2-eq	2.493344	3.626899
Climate change – biogenic	kg CO_2-eq	0.448918	0.650955
Climate change – fossil	kg CO_2-eq	1.93927	2.825364
Resource use, fossils	MJ	65.63016	97.35076
Water use	m^3	1.99894	3.079166

Overall, Route A was more energy-efficient per batch of casticin produced, whereas Route B offered meaningful valorization of herbal residues that would otherwise be discarded. Process optimization – including ethanol recycling, heat integration, or renewable electricity – could markedly improve the sustainability profile of Route B.

In summary, the per-batch assessment highlights clear trade-offs in residue valorization: Route B improves material-efficiency metrics by reducing solvent mass and utilizing a waste stream, whereas energy-related indicators increase due to additional drying/extraction steps. Route B remains a practical valorization option, but its environmental advantage is not unconditional under the present assumptions. Instead, the analysis identifies improvement levers (solvent recovery, heat integration, and electricity source) that would be required to translate improved material efficiency into reduced life-cycle impacts.

3.5.2 Greenness metrics (PMI and *E*-factor)

3.5.2.1 Process mass intensity (PMI) and E-factor. On a per-batch basis, Route B decreased PMI from 1925 to 1409 and *E*-factor from 1921 to 1407, indicating substantially improved material efficiency. These metrics reflect total resource input and waste generation relative to isolated product and are widely used for green-chemistry benchmarking.[26,58]

Route A showed higher PMI due to large solvent volumes and three-stage maceration using 60% ethanol (>104 L). In contrast, Route B used UAE with 70% ethanol (1.4 L per 100 g residue), achieving significant reductions in solvent and water requirements.[56,57] Despite UAE consuming 0.25 kWh of electricity, its process intensification effect lowered overall PMI, consistent with prior reports showing up to 50% PMI reduction *versus* maceration.[56,59,60]

The *E*-factor followed a similar trend: Route B generated less waste relative to product (1407 *vs.* 1921), aided by lower solvent mass and higher product recovery (0.11% *vs.* 0.104%). Importantly, using post-distillation residue avoids additional biomass extraction, improving circularity and reducing ecological harvesting pressure.

Together, PMI and *E*-factor (Table 7), combined with LCA metrics (Tables 5 and 6), reveal a clear mass – *vs.* – energy trade-off between the two routes.

3.5.3 Interpretation: mass-*vs*-energy trade-off and improvement levers. PMI and *E*-factor strongly favor Route B due to its superior material efficiency and residue valorization. LCA indicators, however, show that Route A performs slightly better in energy-related emissions. This reflects the broader challenge in sustainable process design: balancing mass efficiency with energy demand.[26,52,58,61]

Route B remains a practical valorization option, but its environmental advantage is not unconditional under the present assumptions. Instead, the analysis identifies improvement levers (solvent recovery, heat integration, and electricity source) that would be required to translate improved material efficiency into reduced life-cycle impacts.[10,12,62–64]

Sensitivity check (screening-level): a ±20% variation in electricity consumption was applied as a simple robustness scenario; energy-related impact indicators scale proportionally and did not change the qualitative route comparison. Likewise, assuming a ±20% variation in solvent recovery/loss affects PMI and *E*-factor proportionally but does not reverse the observed mass-energy trade-off. Therefore, within reasonable laboratory-scale uncertainty bounds, the comparative trends are stable,

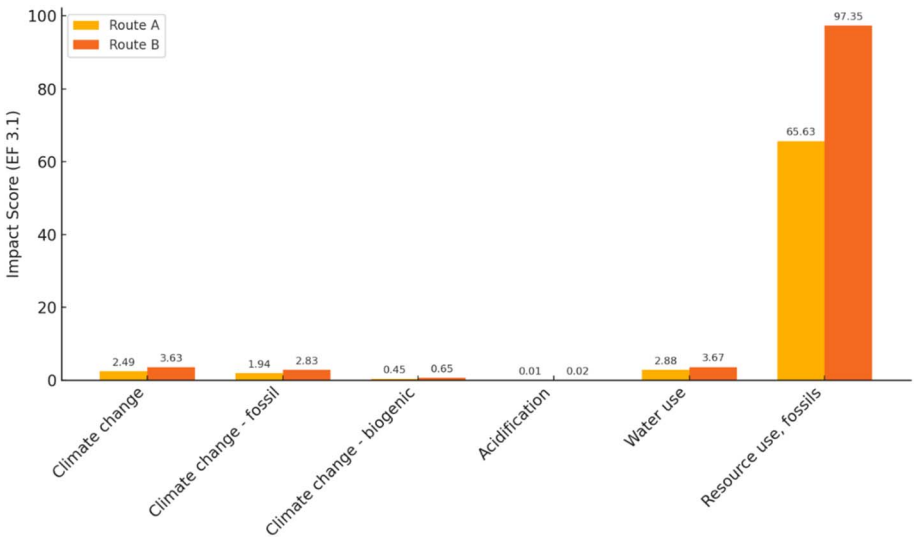

Fig. 8 Comparative per-batch impacts (climate change, fossil resource use, water use) for Route A and Route B under the stated system boundaries and assumptions.

Table 7 Comparison of PMI and *E*-factor for two extraction routes of casticin

Parameter	Route A (raw fruit)	Route B (post-distillation residue)
PMI	1925	1409
E-factor	1921	1407
Extraction type	Maceration	UAE (ultrasound-assisted extraction)
Solvent volume	104.4 L	1.4 L
Yield (%)	0.104%	0.11%

while absolute values would require a more rigorous, product-normalized LCA.

Overall, the environmental assessment highlights a meaningful trade-off between resource efficiency and energy burden in waste-based extraction. The integrated use of mass-intensity, waste-generation, and life-cycle metrics provides a comprehensive evaluation of greenness and identifies actionable levers for process improvement.

Specific improvement levers that could markedly reduce the environmental footprint of Route B include: (1) solvent recovery and recycling (could reduce ethanol demand by 70–80%), (2) heat integration between distillation and drying operations, (3) renewable or grid-decarbonized electricity for UAE, (4) process intensification to minimize residue drying requirements.

4. Discussion

4.1. Comparison of chemical composition with previous reports

Previous studies on *Vitex rotundifolia* have predominantly focused on the volatile fraction/essential oil, with GC–MS being the principal analytical tool Hu *et al.* reported that the volatile fraction of *V. rotundifolia* is dominated by mono- and sesquiterpenes, reflecting the chemical characteristics of essential oils but providing limited information on non-volatile metabolites of medium to high polarity.[50] Similarly, Kim described moderate anti-inflammatory activity associated mainly with volatile constituents.[2]

In contrast, phytochemical investigations and comprehensive reviews have consistently emphasized that flavonoids, iridoid glycosides and labdane/abietane-type diterpenoids represent the key bioactive constituents of the genus *Vitex*.[38,65,66] Representative compounds such as vitexin, orientin, aucubin and vitexilactone have been isolated from fruits, twigs or leaves of *V. rotundifolia* and shown to exhibit pronounced antioxidant or anti-inflammatory activities.[7,39,67]

Within this context, the untargeted LC-MS/MS profiling performed in the present study demonstrates that the post-distillation residue of *V. rotundifolia* retains a chemically rich metabolite spectrum, including flavonoids, phenolic acids, iridoid glycosides and non-volatile diterpenoids. These findings broaden the experimental evidence that non-volatile, medium-to-high polarity metabolites remain in the post-distillation residue and can be recovered under condition-matched extraction, complementing earlier studies focused primarily on essential oils.

4.2. Chemical basis of antioxidant and anti-inflammatory activities

The LC-MS/MS dereplication is consistent with the extract-level antioxidant and NO-inhibitory screening activities observed for R70; however, the present data do not establish specific molecular mechanisms.[68] Flavonoids and phenolic acids, which constitute a significant portion of the annotated metabolites, are well known for their ability to scavenge free radicals, stabilize reactive oxygen and nitrogen species, and is often associated with oxidative stress – an upstream driver of inflammatory responses. Kim (2009) and Le (2022) demonstrated that polyphenol-rich fractions from *V. rotundifolia* simultaneously exhibit strong radical-scavenging capacity and NO inhibition in LPS-stimulated RAW264.7 macrophages.[6,7]

Moreover, the concomitant presence of multiple metabolite classes (*e.g.*, flavonoids, iridoid glycosides, and terpenoids) may contribute to the observed activities through complementary or additive effects, a common feature of complex botanical extracts. Consistent with prior reports on *V. rotundifolia*, whole extracts can modulate inflammatory markers *in vitro*, supporting a multi-target mode of action rather than the effect of a single dominant compound. In the present study, synergistic effects were not experimentally tested in this study; dedicated combination experiments would be required to demonstrate true synergy.[38,39,65]

4.3. Implications for a dual-output biorefinery approach

From a chemical and process perspective, the present findings support an integrated utilization concept in which *V. rotundifolia* biomass can deliver (i) essential oil as a volatile product stream and (ii) a residue-derived extract rich in non-volatile bioactives. This concept is aligned with residue valorization and resource efficiency, while the net environmental benefit depends on process conditions and energy management.[6,39,67]

This integrated utilization strategy broadens the chemical understanding of *V. rotundifolia* across volatile and non-volatile fractions and provides a basis for designing residue-utilization workflows with explicitly quantified trade-offs and transparent assumptions.

5. Conclusion

This study shows that post-distillation residues of *Vitex rotundifolia* remain chemically rich and retain extract-level antioxidant and NO-inhibitory activities, supporting their valorization as a secondary feedstock for recovering non-volatile constituents. R70 was selected as the most balanced residue-derived extract under the tested conditions, and untargeted UHPLC-QTOF-MS/MS provided curated tentative annotation of 88 metabolites, with representative known constituents isolated and structurally confirmed. A comparative greenness screening indicates improved mass-based metrics for the residue-based route but higher per-batch energy-related impacts,

underscoring that sustainability conclusions are condition-dependent and should be evaluated with transparent inventory assumptions and, where possible, yield-normalized functional units.

Author contributions

Kieu Dang Minh Nhut, Dao Pham Duy Quang, Tran Hoai Cuong: investigation, data analysis. Nguyen Thi Nhu Quynh, Cao Van Du: data analysis, data curation. Pham Thi Nhat Trinh: writing – review & editing, conceptualization, LC-MS/MS analysis. Phung Van Trung: investigation, NMR spectral analysis, writing – original draft. Le Tien Dung: writing – review & editing, supervision, conceptualization.

Conflicts of interest

The authors declare that none of the work described in this research has been impacted by any known conflicting financial interests or personal relationships.

Data availability

The data supporting the findings of this study are available within the article and its supplementary information (SI). Supplementary information: NMR spectra of the isolated compounds (**VR1–VR4**), GC-MS data of the essential oil, LC-MS/MS annotation tables, statistical analyses (PCA and correlation matrices), cell viability data, and environmental assessment datasets. See DOI: https://doi.org/10.1039/d5ra09731b.

Acknowledgements

The authors also sincerely thank Ecochain for providing a 7-day free trial of the Mobius LCA platform, which enabled the completion of the environmental impact assessment presented in this research. This project was supported by the Vietnam Academy of Science and Technology (VAST) under the Excellent Research Group Development Program NCXS02.03/25-26 (VAST).

References

1 S. Ganapaty and K. N. Vidyadhar, *J. Nat. Remedies*, 2005, **5**, 75–95.
2 C. Kim, H. J. Bu, S. J. Lee, C. Gu Hyun and N. Ho Lee, *J. Appl. Pharm. Sci.*, 2014, **4**, 12–15.
3 Y. A. Kim, H. Kim and Y. Seo, *Nat. Prod. Commun.*, 2013, **8**, 1405–1408.
4 D. Le, S. Han, K. H. Min and M. Lee, *Metabolites*, 2023, **13**, 249.
5 J.-L. Yao, S.-M. Fang, R. Liu, M. Oppong, E.-W. Liu, G.-W. Fan and H. Zhang, *Molecules*, 2016, **21**, 1179.
6 D. Le, S. Han, J. Ahn, J. Yu, C.-K. Kim and M. Lee, *Antioxidants*, 2022, **11**, 454.
7 D.-K. Kim, *Biomol. Ther.*, 2009, **17**, 412–417.
8 T. H. Thai, P. T. Hong and D. T. Minh, *Tap. Chi Sinh Hoc*, 2006, **28**(4), 93–95.
9 H. T. VAN, V. T. H. TRAN, N. H. N. TON, T. N. LUU, N. T. A. HUYNH and V. S. LE, *Banats J. Biotechnol.*, 2020, **11**, 22–29.
10 P. T. Anastas and J. C. Warner, *Green Chemistry*, Oxford University PressOxford, 2000.
11 ACS Green Chemistry Institute, *Twelve Principles of Green Chemistry*, American Chemical Society, 1998, https://www.acs.org/green-chemistry-sustainability/principles/12-principles-of-green-chemistry.html.
12 International Sustainable Chemistry Collaborative Centre (ISC3), *Key Characteristics of Sustainable Chemistry*, ISC3, 2021.
13 R. P. Adams, *Identification of Essential Oil Components by Gas Chromatography/Mass Spectrometry*, Allured Publishing, Carol Stream, IL, 4th edn, 2007.
14 F. Chemat, N. Rombaut, A.-G. Sicaire, A. Meullemiestre, A.-S. Fabiano-Tixier and M. Abert-Vian, *Ultrason. Sonochem.*, 2017, **34**, 540–560.
15 L. Fu, B.-T. Xu, X.-R. Xu, R.-Y. Gan, Y. Zhang, E.-Q. Xia and H.-B. Li, *Food Chem.*, 2011, **129**, 345–350.
16 J. Zhishen, T. Mengcheng and W. Jianming, *Food Chem.*, 1999, **64**, 555–559.
17 M. S. Blois, *Nature*, 1958, **181**, 1199–1200.
18 R. Re, N. Pellegrini, A. Proteggente, A. Pannala, M. Yang and C. Rice-Evans, *Free Radic. Biol. Med.*, 1999, **26**, 1231–1237.
19 L. C. Green, D. A. Wagner, J. Glogowski, P. L. Skipper, J. S. Wishnok and S. R. Tannenbaum, *Anal. Biochem.*, 1982, **126**, 131–138.
20 T. Mosmann, *J. Immunol. Methods*, 1983, **65**, 55–63.
21 H. Horai, M. Arita, S. Kanaya, Y. Nihei, T. Ikeda, K. Suwa, Y. Ojima, K. Tanaka, S. Tanaka, K. Aoshima, Y. Oda, Y. Kakazu, M. Kusano, T. Tohge, F. Matsuda, Y. Sawada, M. Y. Hirai, H. Nakanishi, K. Ikeda, N. Akimoto, T. Maoka, H. Takahashi, T. Ara, N. Sakurai, H. Suzuki, D. Shibata, S. Neumann, T. Iida, K. Tanaka, K. Funatsu, F. Matsuura, T. Soga, R. Taguchi, K. Saito and T. Nishioka, *J. Mass Spectrom.*, 2010, **45**, 703–714.
22 MoNA (MassBank of North America), MassBank of North America spectral database, https://mona.fiehnlab.ucdavis.edu/.
23 E. L. Schymanski, J. Jeon, R. Gulde, K. Fenner, M. Ruff, H. P. Singer and J. Hollender, *Environ. Sci. Technol.*, 2014, **48**, 2097–2098.
24 M. Sharar, E. M. Saied, M. C. Rodriguez, C. Arenz, M. Montes-Bayón and M. W. Linscheid, *Anal. Bioanal. Chem.*, 2017, **409**, 2015–2027.
25 C. Jimenez-Gonzalez, C. S. Ponder, Q. B. Broxterman and J. B. Manley, *Org. Process Res. Dev.*, 2011, **15**, 912–917.
26 R. A. Sheldon, *Green Chem.*, 2007, **9**, 1273.
27 F. Piccinno, R. Hischier, S. Seeger and C. Som, *J. Clean. Prod.*, 2018, **174**, 283–295.
28 J. Dai and R. J. Mumper, *Molecules*, 2010, **15**, 7313–7352.
29 A. Wojdylo, J. Oszmianski and R. Czemerys, *Food Chem.*, 2007, **105**, 940–949.

30 A. R. Alzahrani, N. Hosny, D. I. Mohamed, H. H. Abo Nahas, A. Albogami, T. M. I. Al-Hazani, I. A. A. Ibrahim, A. H. Falemban, G. A. Bamagous and E. M. Saied, *RSC Adv.*, 2024, **14**, 19400–19427.
31 D. Turcov, A. S. Barna, O. T. Apreutesei Ciuperca, A. Trifan, A. C. Puitel and D. Suteu, *Bioresources*, 2022, **17**, 4730–4744.
32 M. Irakli, E. Bouloumpasi, S. Christaki, A. Skendi and P. Chatzopoulou, *Antioxidants*, 2023, **12**, 549.
33 E. Bouloumpasi, M. Hatzikamari, S. Christaki, A. Lazaridou, P. Chatzopoulou, C. G. Biliaderis and M. Irakli, *Processes*, 2024, **12**, 140.
34 R. Schmid, S. Heuckeroth, A. Korf, A. Smirnov, O. Myers, T. S. Dyrlund, R. Bushuiev, K. J. Murray, N. Hoffmann, M. Lu, A. Sarvepalli, Z. Zhang, M. Fleischauer, K. Dührkop, M. Wesner, S. J. Hoogstra, E. Rudt, O. Mokshyna, C. Brungs, K. Ponomarov, L. Mutabdžija, T. Damiani, C. J. Pudney, M. Earll, P. O. Helmer, T. R. Fallon, T. Schulze, A. Rivas-Ubach, A. Bilbao, H. Richter, L.-F. Nothias, M. Wang, M. Orešič, J.-K. Weng, S. Böcker, A. Jeibmann, H. Hayen, U. Karst, P. C. Dorrestein, D. Petras, X. Du and T. Pluskal, *Nat. Biotechnol.*, 2023, **41**, 447–449.
35 M. M. Yousef, A.-N. A. Zohri, A. M. G. Darwish, A. Shamseldin, S. A. Kabeil, A. Abdelkhalek, R. Binsuwaidan, M. Jaremko, H. A. Alshwyeh, E. E. Hafez and E. M. Saied, *Front. Microbiol.*, 2023, **14**, 1219823.
36 M. Ono, M. Yamamoto, T. Yanaka, Y. Ito and T. Nohara, *Chem. Pharm. Bull.*, 2001, **49**, 82–86.
37 D.-K. Kim, *Biol. Ther.*, 2009, **17**, 412–417.
38 N. Azizul, W. Ahmad, W. Amir Nizam, W. Ahmad, N. Rosli, M. Aniq, H. Azmi, C. Liang, N. W. Mazlan and S. Assaw, *Tradit. Med. Res.*, 2021, **6**, 1–10.
39 C. Lee, J. W. Lee, Q. Jin, H. J. Lee, S.-J. Lee, D. Lee, M. K. Lee, C. K. Lee, J. T. Hong, M. K. Lee and B. Y. Hwang, *Bioorg. Med. Chem. Lett.*, 2013, **23**, 6010–6014.
40 E. A. Ahmed, M. O. El-Derany, A. M. Anwar, E. M. Saied and S. Magdeldin, *Int. J. Mol. Sci.*, 2022, **24**, 210.
41 S. E. Elshaer, G. M. Hamad, S. E. Sobhy, A. M. G. Darwish, H. H. Baghdadi, H. H. Abo Nahas, F. M. El-Demerdash, S. S. A. Kabeil, A. S. Altamimi, E. Al-Olayan, M. Alsunbul, O. K. Docmac, M. Jaremko, E. E. Hafez and E. M. Saied, *Front. Pharmacol*, 2024, **15**, 1378249.
42 O. Kunert, F. Alperth, E. Pabi and F. Bucar, *Heliyon*, 2023, **9**, e22309.
43 G. L. Dong, J. R. Min, C. Sunghun, S. C. Ha and L. Sanghyun, *Nat. Prod. Sci.*, 2014, **20**, 206–210.
44 C. A. Rice-Evans, N. J. Miller and G. Paganga, *Free Radic. Biol. Med.*, 1996, **20**, 933–956.
45 J.-H. Yoon and S. J. Baek, *Yonsei Med. J.*, 2005, **46**, 585.
46 C. Santangelo, R. Varì, B. Scazzocchio, R. Di Benedetto, C. Filesi and R. Masella, *Ann. Ist. Super. Sanita*, 2007, **43**, 394–405.
47 A. N. Panche, A. D. Diwan and S. R. Chandra, *J. Nutr. Sci.*, 2016, **5**, e47.
48 B. T. Lam, H. T. Ly, H. T. Tran and V. M. Le, *Pharmacol. Res.*, 2025, **15**, 100608.
49 J.-Y. Kim and S. H. Shim, *Biomolecules*, 2019, **9**, 727.
50 Y. Hu, T.-T. Hou, H.-L. Xin, Q.-Y. Zhang, H.-C. Zheng, K. Rahman and L.-P. Qin, *Indian J. Med. Res.*, 2007, **126**, 68–72.
51 J. Vanneste, T. Van Gerven, E. Vander Putten, B. Van der Bruggen and L. Helsen, *Sci. Total Environ.*, 2011, **409**, 3595–3602.
52 R. A. Sheldon, *Chem. – Eur. J.*, 2024, **30**, e202402207.
53 W. Liu, Z. Zhang, X. Xie, Z. Yu, K. von Gadow, J. Xu, S. Zhao and Y. Yang, *Sci. Rep.*, 2017, **7**, 39857.
54 B. Shumeiko, M. Auersvald, D. Vrtiška, P. Straka, P. Šimáček, I. Svetlik, S. Bezergianni and D. Kubička, *Chem. Eng. J.*, 2023, **465**, 142899.
55 K. Lan, L. Ou, S. Park, S. S. Kelley, P. Nepal, H. Kwon, H. Cai and Y. Yao, *Biotechnol. Biofuels*, 2021, **14**, 191.
56 F. Chemat, M. A. Vian and G. Cravotto, *Int. J. Mol. Sci.*, 2012, **13**, 8615–8627.
57 E. M. M. Flores, G. Cravotto, C. A. Bizzi, D. Santos and G. D. Iop, *Ultrason. Sonochem.*, 2021, **72**, 105455.
58 F. Roschangar, R. A. Sheldon and C. H. Senanayake, *Green Chem.*, 2015, **17**, 752–768.
59 J. A. Okolie, E. I. Epelle, M. E. Tabat, U. Orivri, A. N. Amenaghawon, P. U. Okoye and B. Gunes, *Process Saf. Environ. Prot.*, 2022, **159**, 323–344.
60 M. D. Esclapez, J. V. García-Pérez, A. Mulet and J. A. Cárcel, *Food Eng. Rev.*, 2011, **3**, 108–120.
61 X. Wang, Y. Wei, Z. Fan, Y. Chen and Z. Cui, *Sci. Total Environ.*, 2024, **922**, 171319.
62 B. Häussling Löwgren, C. Hoffmann, M. G. Vijver, B. Steubing and G. Cardellini, *J. Clean. Prod.*, 2025, **491**, 144831.
63 L. Mandi, S. Hilali, F. Chemat and A. Idlimam, in *Green Food Processing Techniques*, Elsevier, 2019, pp. 499–511.
64 R. Mahmud, S. M. Moni, K. High and M. Carbajales-Dale, *J. Clean. Prod.*, 2021, **317**, 128247.
65 N. Kamal, N. S. Mio Asni, I. N. A. Rozlan, M. A. H. Mohd Azmi, N. W. Mazlan, A. Mediani, S. N. Baharum, J. Latip, S. Assaw and R. A. Edrada-Ebel, *Plants*, 2022, **11**, 1944.
66 S. Ganapaty and K. N. Vidyadhar, *J. Nat. Remedies*, 2005, **5**, 75–95.
67 M. Ono, Y. Ito and T. Nohara, *Phytochemistry*, 1998, **48**, 207–209.
68 A. Elkelish, A. M. Abu-Elsaoud, A. M. Alqahtani, M. El-Nablaway, N. Al harthi, N. Al harthi, S. Lakoh, E. M. Saied and M. Labib, *BMC Complementary Med. Ther.*, 2024, **24**, 413.